

---

# A light curve model of V2491 Cyg: Classical nova outburst on a cool and massive white dwarf

Mariko KATO<sup>1</sup>, Hideyuki SAIO,<sup>2</sup> and Izumi HACHISU<sup>3</sup>

<sup>1</sup>Department of Astronomy, Keio University, Hiyoshi, Yokohama 223-8521, Japan

<sup>2</sup>Astronomical Institute, Graduate School of Science, Tohoku University, Sendai, 980-8578, Japan

<sup>3</sup>Department of Earth Science and Astronomy, College of Arts and Sciences, The University of Tokyo, 3-8-1 Komaba, Meguro-ku, Tokyo 153-8902, Japan

\*E-mail: mariko.kato@hc.st.keio.ac.jp

Received ; Accepted

## Abstract

The classical nova V2491 Cyg was once suggested to be a recurrent nova. We have broadly reproduced the light curve of V2491 Cyg by a nova outburst model on a cold  $1.36 M_{\odot}$  white dwarf (WD), which strongly suggests that V2491 Cyg is a classical nova outbursting on a cold very massive WD rather than a recurrent nova outbursting on a warmer WD like the recurrent nova RS Oph. In a long-term evolution of a cataclysmic binary, an accreting WD has been settled down to a thermal equilibrium state with the balance of gravitational energy release and neutrino loss. The central temperature of the WD is uniquely determined by the energy balance. The WD is hot (cold) for a high (low) mass-accretion rate. We present the central temperatures, ignition masses, ignition radii, and recurrence periods for various WD masses and mass-accretion rates. In a classical nova, which corresponds to a low mass-accretion rate, the WD is cool and strongly degenerated and the ignition mass is large, which result in a strong nova outburst. In a recurrent nova, the WD is relatively warmer because of a high mass accretion rate and the outburst is relatively weaker. The gravitational energy release substantially contributes to the luminosity during the recurrent nova outbursts. We compare physical properties between classical novae and recurrent novae and discuss the essential differences between them.

**Key words:** novae, cataclysmic variables — stars: individual (V2491 Cyg, RS Oph) — white dwarfs — X-rays: binaries

---

## 1 Introduction

A nova occurs on an accreting white dwarf (WD) in a cataclysmic binary system. When the accreted H-rich matter reaches a critical value (ignition mass) hydrogen thermonuclear runaway sets in, which triggers a nova outburst. The envelope expands to a giant size and strong wind mass-loss occurs. The optical brightness quickly rises to maximum

followed by a gradual decrease. After the wind stops, the WD enters the supersoft X-ray source (SSS) phase that continues until the hydrogen burning extinguishes.

Kato (1983) proposed an idea that the nova decay phase can be followed by a sequence of steady-state solutions. In nova outbursts, winds are accelerated deep inside the photosphere. Based on the optically thick wind theory together with the OPAL opacity (Iglesias & Rogers

1996), Kato & Hachisu (1994) systematically calculated nova outburst evolutions for various WD masses and chemical compositions. Using their results, many nova light curves have been calculated, which are in good agreement with observed light curves for a number of classical novae (Hachisu & Kato 2006; Hachisu & Kato 2015; Hachisu & Kato 2016a; Hachisu & Kato 2018a; Hachisu & Kato 2018b; Hachisu & Kato 2019b; Hachisu & Kato 2021). In these models, optical/IR light curves are followed by the free-free emission light curves based on the wind mass-loss rates obtained with the optically thick wind theory. After the wind stops, the SSS phase can be followed by the sequence of static solutions. Good agreements of theoretical with observed light curves indicate that the steady-state assumption in the optically thick winds can be well applied to the decay phase of a classical nova.

The timescale of a nova outburst evolution depends strongly on the WD mass but weakly on the chemical composition of the envelope. Thus, the decline rate in the optical light curve and duration of a SSS phase give a rough estimate of the WD mass. In general a fast (slow) nova corresponds to a massive (less massive) WD (e.g., Hachisu et al. (2020)). Both the optical and SSS phases have been theoretically calculated for various WD masses and envelope chemical compositions (Kato & Hachisu 1994; Kato 1999; Sala & Hernanz 2005; Hachisu & Kato 2006; Wolf et al. 2013; Kato et al. 2013; Hachisu & Kato 2015; Hachisu & Kato 2018b; Hachisu & Kato 2019b; Kato et al. 2020; Hachisu & Kato 2021). The overall light curves of IR/optical and SSS phases are well reproduced with the optically thick wind theory for a number of classical novae (Kato & Hachisu 1994; Kato 1999; Hachisu & Kato 2006; Kato et al. 2013; Hachisu & Kato 2015; Hachisu & Kato 2018b; Hachisu & Kato 2019b; Hachisu & Kato 2021).

V2491 Cyg outbursted in 2008 (Nakano et al. 2008). Its optical light curve shows a rapid decline followed by a plateau-like phase, resembling those of recurrent novae. The short SSS phase suggests a very massive WD. Ness et al. (2011) pointed out the strong similarity of X-ray spectrum in V2491 Cyg and the recurrent nova RS Oph. Page et al. (2010) and Pagnotta & Schaefer (2014) discussed that V2491 Cyg is possibly a recurrent nova (see, also, Tomov et al. (2008)). Hachisu & Kato (2019a) compared the light curves of V2491 Cyg and RS Oph, both of which show a similar X-ray emergence time (see their figure 16). These similarities suggest that both RS Oph and V2491 Cyg host a massive WD ( $\sim 1.35 M_{\odot}$ : see the next section). On the other hand, it was suggested that V2491 Cyg should be a classical nova, because (1) a heavy element enrichment is detected in its ejecta (Munari et al. 2011),

which is a characteristic property of classical novae, and also because (2) V2491 Cyg seems to be an intermediate polar (IP) (Takei et al. 2009; Takei et al. 2011; Zemko et al. 2015; Sun et al. 2020) whereas no recurrent novae have been identified as an IP.

Kato & Hachisu (2020) found a statistical difference between classical novae and recurrent novae in the  $t_{\text{off}} - t_{\text{SSS}}$  diagram in which recurrent novae have a longer SSS duration than classical novae do. Here  $t_{\text{off}}$  is the X-ray turnoff time, which indicates the total duration of the outburst, and  $t_{\text{SSS}}$  is the SSS duration. They showed that the recurrent nova RS Oph is on the trend of recurrent nova relation, and V2491 Cyg is on the classical nova relation. These two novae show a similar X-ray turn-on time but different SSS durations.

In the present paper, we clarify the reason for the different SSS durations between the classical novae and recurrent novae both having similar WD masses. The main difference between them is the mass accretion rate. Thus, we have calculated the interior structure of accreting WDs for various mass-accretion rates.

This paper is organized as follows. Section 2 lists the resemblance and difference between the observational light curves of RS Oph and V2491 Cyg. Section 3 presents our calculation for interior structures of mass accreting WDs for various mass-accretion rates. Based on the results, we present theoretical light curves of V2491 Cyg as a classical nova on a very cold WD in section 4. The light curve is well explained by the optically thick wind theory and additional emission from massive ejecta. In section 5, we study how and why the recurrent nova outbursts are different from the steady-state solutions. Discussion and conclusions follow in sections 6 and 7, respectively.

## 2 Observational Properties of V2491 Cyg and RS Oph

Figure 1 shows the V-band and supersoft X-ray light curves of the classical nova V2491 Cyg (black symbols) as well as those of the recurrent nova RS Oph (red symbols) in the 2006 outburst. For RS Oph, the optical data are taken from Hachisu et al. (2006) and X-ray data are from Hachisu et al. (2007). The optical decline of RS Oph is smooth, followed by a plateau phase. Such an optical light curve is modeled by Hachisu et al. (2006) in which the early decline is mainly described by the free-free emission from optically thin ejecta just outside the photosphere of the WD envelope, whereas the plateau is caused mainly by the photospheric emission from an irradiated optically thick accretion disk. Their model consists of a  $1.35 M_{\odot}$  WD, a large disk with a radius of  $\sim 40 R_{\odot}$  and a red giant

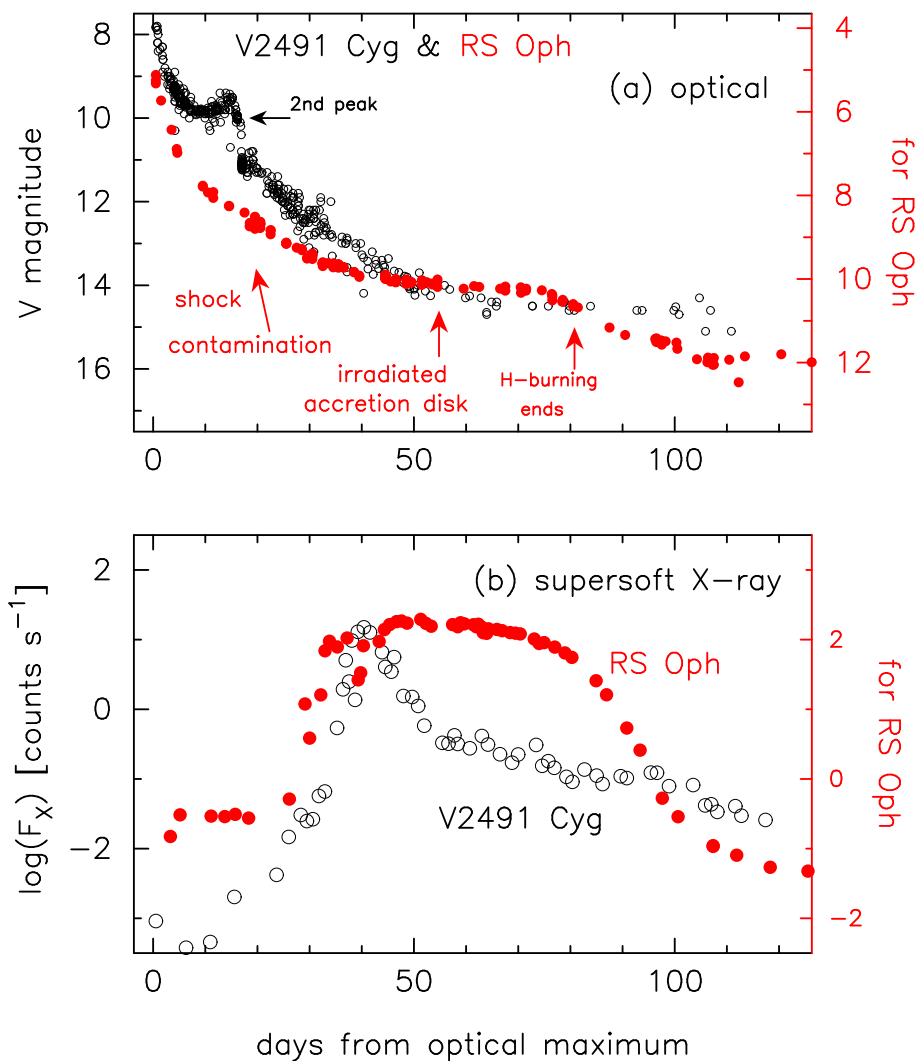


**Fig. 1.** (a) The  $V$  light curves and (b) the supersoft X-ray count rates both for V2491 Cyg (black symbols) and RS Oph (red symbols). The  $V$  light curve of V2491 Cyg is shifted upward by 3.85 mag to match the absolute magnitudes of RS Oph. Also the X-ray count rates of V2491 Cyg are shifted upward by 1.0 dex to match the peak count rates. See the main text for details.

companion. The disk is so large because RS Oph is a symbiotic recurrent nova of orbital period 453.6 days (Brandi et al. 2009) and the separation is as large as  $\sim 300 R_{\odot}$  that permits such a large accretion disk. In classical novae, on the other hand, the orbital period is typically a few to several hours, and the disk is too small to contribute much to the  $V$  light curve. Hachisu et al. (2006) identified the epoch when the hydrogen burning turned off as indicated by a red arrow in figure 1(a). Then, the optical flux decayed faster as the X-ray count rate declines.

We should note that Iijima (2009) differently interpreted that the decay of supersoft X-ray and optical flux in 80–90 days to be the shock breakout from the cool red-giant wind based on his optical spectral analysis of the RS Oph 2006 outburst.

The reddening and distance to RS Oph were obtained

to be  $E(B - V) = 0.65$  mag,  $(m - M)_V = 12.8$  mag and  $d = 1.4$  kpc by Hachisu & Kato (2018b) and Hachisu & Kato (2021). Recently, Hachisu & Kato (2021) examined multiwavelength light curves of RS Oph, and clarified that the  $V$  band light curve of RS Oph is contaminated with shock radiation and thus decays somewhat slower than the pure free-free emission light curve (see their figure 20).

V2491 Cyg, outbursting in 2008, is a fast nova with a moderately bright second peak in its optical light curve. The light curves are plotted in figure 1 (black symbols), the data of which are the same as those in Hachisu & Kato (2009). This object is strongly suggested to be an intermediate polar (IP) (Takei et al. 2009; Takei et al. 2011; Zemko et al. 2015). For the mechanism of the second peak Hachisu & Kato (2009) proposed an idea that stored magnetic energy is released when the mag-

netic energy becomes larger than the rotation energy of the expanding envelope, which should occur in the middle of the optical decline. Hachisu & Kato (2016a) examined V2491 Cyg in the *UBV* color evolution and obtained  $E(B - V) = 0.23$ ,  $(m - M)_V = 16.5$ .  $d = 14$  kpc. These values are revised to be  $E(B - V) = 0.4 \pm 0.05$ ,  $(m - M)_V = 16.65 \pm 0.2$ ,  $d = 12.1 \pm 2$  kpc based on the time-stretched color-magnitude diagram method (Hachisu & Kato 2021).

V2491 Cyg was well observed with X-ray satellites. The X-ray light curve and spectra are reported in detail by Page et al. (2010) and Ness et al. (2011). The X-ray light curve shows a rather shorter ( $\sim 10$  days) bright peak than that of RS Oph, followed by a decline phase. The decline rate (slope) suddenly becomes slower on Day  $\sim 53$ . This change has not been theoretically explained while many novae show a quick decay in the X-ray count rate, e.g., in V1974 Cyg, V382 Vel, and V597 Pup (Hachisu & Kato 2010). X-ray spectra were taken on Day  $\sim 40$  and Day  $\sim 50$  with *XMM-Newton*. Ness et al. (2011) pointed out the remarkable similarity of the X-ray spectra between V2491 Cyg on Day 40.18 and RS Oph on Day 39.7. Also the blackbody temperature  $6.3 \times 10^5$  K of V2491 Cyg on Day 40.18 (Ness et al. 2011) is similar to  $(6.3 - 8.3) \times 10^5$  K of RS Oph on Day 39.7 (Ness et al. 2007). Such similarities suggest that the both novae have similar mass WDs. The mass estimate in the theoretical light curve fittings indicates  $\sim 1.35 M_\odot$  for the both novae. See figure 48 of Hachisu & Kato (2019a) for V2491 Cyg, and figure 3 of Hachisu et al. (2006) for RS Oph.

Figure 1a compares the *V* light curves of the two novae. The *V* light curve of V2491 Cyg are shifted upward by 3.85 mag to match the absolute magnitudes of RS Oph. Here 3.85 mag corresponds to the difference of the two distance moduli, that is,  $(m - M)_V = 16.65$  for V2491 Cyg (Hachisu & Kato 2021) and  $(m - M)_V = 12.8$  for RS Oph (Hachisu & Kato 2018b). V2491 Cyg shows a prominent second peak which has not been observed in recurrent novae. Also the bright optical peak of V2491 Cyg,  $M_V = -9.2$  mag, is much brighter than  $M_V = -8.0$  mag in RS Oph or other recurrent novae (Hachisu & Kato 2018b).

Hachisu et al. (2020) theoretically related the peak brightness ( $M_{V,\max}$ ) and decline time ( $t_3$ ) by 3 mag from the peak to the ignition mass and mass accretion rate (or recurrence period). If we assume that  $M_{V,\max} = -9.2$  and  $t_3 = t_2/0.54 = 4/0.54 = 7.4$  d for V2491 Cyg, their figure 6 indicates that the WD mass is  $M_{\text{WD}} = 1.32 M_\odot$  and the mass accretion rate to the WD is  $\dot{M}_{\text{acc}} = 3 \times 10^{-11} M_\odot \text{ yr}^{-1}$  or the recurrence period is  $P_{\text{rec}} = 1.5 \times 10^5$  yr for solar abundance. These properties indicate that V2491 Cyg is a classical nova rather than a recurrent nova.

After Day 60, the optical light curve of V2491 Cyg becomes flat, resembling to a plateau phase in recurrent novae. The absolute *V* magnitude of the flat phase in V2491 Cyg is slightly fainter than that in RS Oph (see figure 1a). In recurrent novae, the plateau phase is explained by the contribution of an irradiated accretion disk. The plateau phase is brighter for a larger accretion disk. The brightness of plateau is about  $M_V = m_V - (m - M)_V \approx 14.5 - 16.65 = -2.15$  in V2491 Cyg,  $M_V = m_V - (m - M)_V \approx 14.5 - 16.85 = -2.35$  in U Sco (Hachisu & Kato 2021), and  $M_V = m_V - (m - M)_V \approx 10.0 - 12.8 = -2.8$  in RS Oph. This trend simply means that the size of accretion disk is smallest in V2491 Cyg and largest in RS Oph, and the size in U Sco is between them. The orbital period of U Sco is  $P_{\text{orb}} = 1.23$  d, so we expect that the orbital period of V2491 Cyg is probably shorter than a day.

V2491 Cyg is strongly suggested to be a member of intermediate polars (IPs) (Zemko et al. 2015), of which the typical orbital period ranges from a few to several hours.<sup>1</sup> We suppose that the orbital period is a few to several hours and therefore the orbital separation of V2491 Cyg is probably as small as  $\lesssim 1.5 R_\odot$ . A small irradiated accretion disk hardly contributes to the visual band. For example, the recurrent nova U Sco ( $P_{\text{orb}} = 1.23$  d) has an irradiated disk of  $\sim 2 R_\odot$  (Hachisu et al. 2000), of which the contribution to the total brightness is much fainter than that in RS Oph (see e.g., figure 124 in Hachisu & Kato (2019b)).

### 3 Accreting White Dwarfs: Hot or Cool ?

In many nova calculations, the central temperature of the WD and the mass accretion rate are often treated as independent parameters (e.g. Prialnik & Kovetz (1995); Yaron et al. (2005); Starrfield et al. (2012); Wolf et al. (2013); Denissenkov et al. (2013); Chen et al. (2019)). The resultant flash properties depend largely on the WD temperature even if the mass-accretion rate and WD mass are the same. In a long term binary evolution, accreting WDs undergo a number of shell flashes, and their interiors adjust to their mass accretion (for more details, see section 6.3). To clarify the difference between V2491 Cyg and RS Oph, we need to obtain their WD models consistent with their mass-accretion rates, because their WD masses are probably the same or very similar but their mass accretion rates are very different.

We calculate hydrogen shell flash models for each set

<sup>1</sup>The Catalog of IPs and IP Candidates by Right Ascension in <https://asd.gsfc.nasa.gov/Koji.Mukai/iphome/catalog/alpha.html> by K. Mukai (2014). Among 74 IPs and IP candidates listed with its orbital period, only two have the orbital period larger than 10 hr: 47.9 hr (GK Per) and 15.4 hr (V2731 Oph).

of the WD mass and mass accretion rate. To prepare an initial WD interior model, we obtain a thermal equilibrium model of each WD by balancing the heating by mass-accretion with the cooling by neutrino loss. Our calculation method and a part of the results have been already published in Kato et al. (2014), Hachisu et al. (2016), and Hachisu et al. (2020). We obtain the hydrogen-rich envelope mass at ignition,  $M_{\text{ig}}$ , central temperature of the WD,  $T_c$ , and radius of the bottom of hydrogen burning zone,  $R_b$ , at the onset of the shell flash (more exactly, at the epoch when the nuclear burning rate increases to  $L_{\text{nuc}} = 10^6 L_{\odot}$ ). The accreted matter has the solar composition of  $X = 0.7$ ,  $Y = 0.28$ , and  $Z = 0.02$  by mass fraction. Our results are summarized in figures 2, 3, and 4.

### 3.1 Ignition Mass

Figure 2 shows the ignition mass vs. mass accretion rate for various WD masses. The ignition mass is smaller for massive WDs and for high mass-accretion rates. The gravitational energy release rate during a mass accretion phase is larger in more massive WDs and for larger mass-accretion rates, which keeps the envelope warmer to reduce the ignition mass (see Kato et al. (2014) for details). The slope of the ignition mass vs.  $\dot{M}_{\text{acc}}$  line along the same WD mass becomes steeper for  $\dot{M}_{\text{acc}} \gtrsim 10^{-8} M_{\odot} \text{ yr}^{-1}$ , because the envelope is not degenerated in such high mass-accretion rates as shown later, and the envelope is easily heated enough to ignite hydrogen. Note that the shell flash can occur even in a non-degenerate envelope (see Discussion in section 6.2). On the other hand, in low mass-accretion rates, the accretion heating is not effective because the envelope is strongly degenerated and efficient conductive energy transport carries heat away in a long interflash period. Thus, much mass need to be accumulated until it satisfies the ignition condition with help of blanket effect.

The dotted blue lines in figure 2 indicate the recurrence period calculated from  $(M_{\text{ig}} - M_0)/\dot{M}_{\text{acc}}$ , where  $M_0$  is leftover of the hydrogen-rich envelope remained unburnt at the end of the previous outburst. This  $M_0$  is calculated from the sequence of static solutions at the epoch when the hydrogen burning turns off (Kato 1999). The WD radius is assumed to be  $R_b$  in figure 4. In low mass accretion rates, the recurrence period is approximately equal to  $M_{\text{ig}}/\dot{M}_{\text{acc}}$  because  $M_0$  is much smaller than  $M_{\text{ig}}$ . The recurrent novae correspond to high mass-accretion rates  $\dot{M}_{\text{acc}} \sim 10^{-7} M_{\odot} \text{ yr}^{-1}$ , whereas the classical novae to  $\dot{M}_{\text{acc}} = 10^{-11}$  to  $10^{-8} M_{\odot} \text{ yr}^{-1}$ .

The two red circles in figure 2 denote the ignition masses taken from our successive hydrogen flash models of a  $1.38 M_{\odot}$  WD with  $\dot{M}_{\text{acc}} = 1.6 \times 10^{-7} M_{\odot} \text{ yr}^{-1}$ . The

lower circle is for the 10th flash (Kato et al. 2017a), in which  $M_{\text{ig}} = 2.0 \times 10^{-7} M_{\odot}$ , and  $P_{\text{rec}} = 0.95 \text{ yr}$ . The upper circle is for the last hydrogen flash (the 1543th flash) before the helium shell flash occurs,  $M_{\text{ig}} = 2.1 \times 10^{-7} M_{\odot}$  and  $P_{\text{rec}} = 0.91 \text{ yr}$ . Both of them locate very close to the line of our  $1.38 M_{\odot}$  WD, because the flash properties are hardly changed during the evolution.

Figure 2 tells us a difference between the classical novae and recurrent novae with the same WD mass. For example, in a  $1.35 M_{\odot}$  WD with  $\dot{M}_{\text{acc}} = 5 \times 10^{-8} M_{\odot} \text{ yr}^{-1}$  ( $P_{\text{rec}} = 12 \text{ yr}$ ), the ignition mass of a recurrent nova is  $M_{\text{ig}} = 7.05 \times 10^{-7} M_{\odot}$ . On the other hand, a classical nova of  $1.0 \times 10^{-9} M_{\odot} \text{ yr}^{-1}$  ( $P_{\text{rec}} = 1650 \text{ yr}$ ), the ignition mass is  $M_{\text{ig}} = 1.65 \times 10^{-6} M_{\odot}$ , 2.3 times larger than the recurrent nova. In an extremely low mass-accretion rate,  $\dot{M}_{\text{acc}} = 1.0 \times 10^{-11} M_{\odot} \text{ yr}^{-1}$  ( $P_{\text{rec}} = 2.48 \times 10^5 \text{ yr}$ ), the ignition mass  $M_{\text{ig}} = 2.48 \times 10^{-6} M_{\odot}$  is 4.5 times larger than that of the recurrent nova. These larger ignition masses guarantee massive ejecta. Because the optical  $V$  peak is brighter for massive ejecta (Hachisu et al. (2020) and section 4.2 in the present paper), a classical nova is much brighter than a recurrent nova in its optical peak even if the WD masses are the same.

### 3.2 White Dwarf Temperature

Figure 3 summarizes the temperature at the center of the WD,  $T_c$ , against various WD masses and mass-accretion rates. The central temperature is determined from a thermal balance between the gravitational energy release owing to mass-accretion and neutrino loss. The core temperature is higher for a larger mass-accretion rate. The slope of  $\Delta \log T_c / \Delta \log \dot{M}_{\text{acc}}$  is moderate for  $\dot{M}_{\text{acc}} > 10^{-8} M_{\odot} \text{ yr}^{-1}$  because neutrino loss increases with the temperature.

The black encircled plus symbol denotes the central temperature of the  $1.38 M_{\odot}$  WD model with  $\dot{M}_{\text{acc}} = 1.6 \times 10^{-7} M_{\odot} \text{ yr}^{-1}$  after it experienced successive 10 and 1543 hydrogen flashes in our long-term calculation (Kato et al. 2017a; Kato et al. 2017b). Starting with the steady-state (thermal equilibrium) model, the central temperature did not change during the series of shell flashes. Thus, the central temperatures at the two epochs are identical. This point lies on our theoretical  $1.38 M_{\odot}$  WD line in figure 3. Note that the core temperature hardly changes during one cycle of shell flash even when the temperature at the nuclear burning region undergoes a cyclic change between  $\log T \text{ (K)} = 7.68$  and  $8.25$ .

The blue crosses and red triangles are the WD temperatures adopted in shell flash calculations (Priyalnik & Kovetz 1995; Yaron et al. 2005; Chen et al. 2019), which will be discussed in section 6.3.

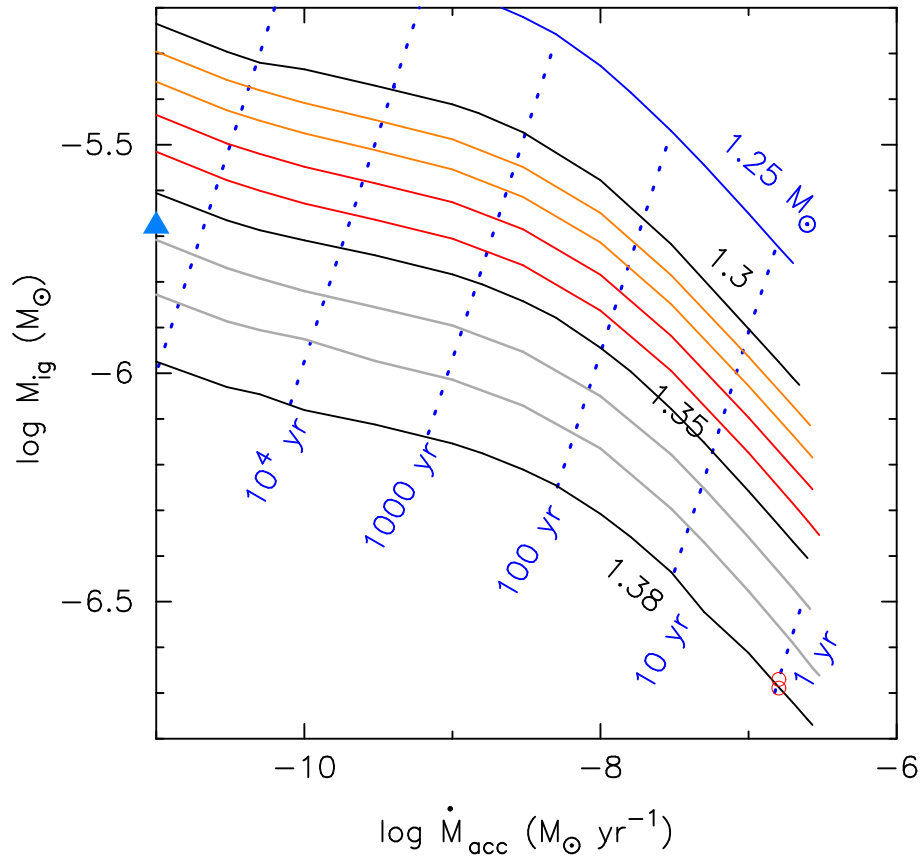


**Fig. 2.** The ignition mass vs. mass accretion rate for the WD mass of, from upper to lower, 1.25 (blue line), 1.3 (black), 1.31 and 1.32 (orange), 1.33 and 1.34 (red), 1.35 (black), 1.36 and 1.37 (gray), and 1.38 (black)  $M_{\odot}$ . The two red open circles indicate the ignition mass of evolution model of 1.38  $M_{\odot}$  with  $\dot{M}_{\text{acc}} = 1.6 \times 10^{-7} M_{\odot} \text{ yr}^{-1}$  at the 10th flash (lower) (Kato et al. 2017a) and 1543th flash (upper) (Kato et al. 2017b). The filled blue triangle indicates the envelope mass at the optical peak of the light curve model of V2491 Cyg (section 4.2). The dotted blue line connects loci at which the recurrence period  $P_{\text{rec}}$  is constant.

### 3.3 Radii of Accreting White Dwarfs

Figure 4 shows the radius of the bottom of the H-rich envelope at the beginning of a hydrogen shell flash. In general, the WD radius is smaller in a more massive WD, and rapidly decreases as the WD mass approaches the Chandrasekhar mass limit. The radius in figure 4 follows this tendency and, in addition, it shows a dependence on the mass-accretion rate. The radius is slightly larger for a larger mass-accretion rate because the WD is warmer by a larger gravitational energy release rate. Comparing a classical nova with a recurrent nova having the same WD mass, we expect slightly stronger shell flashes in low mass-accretion rates because the surface gravity is stronger in a smaller radius.

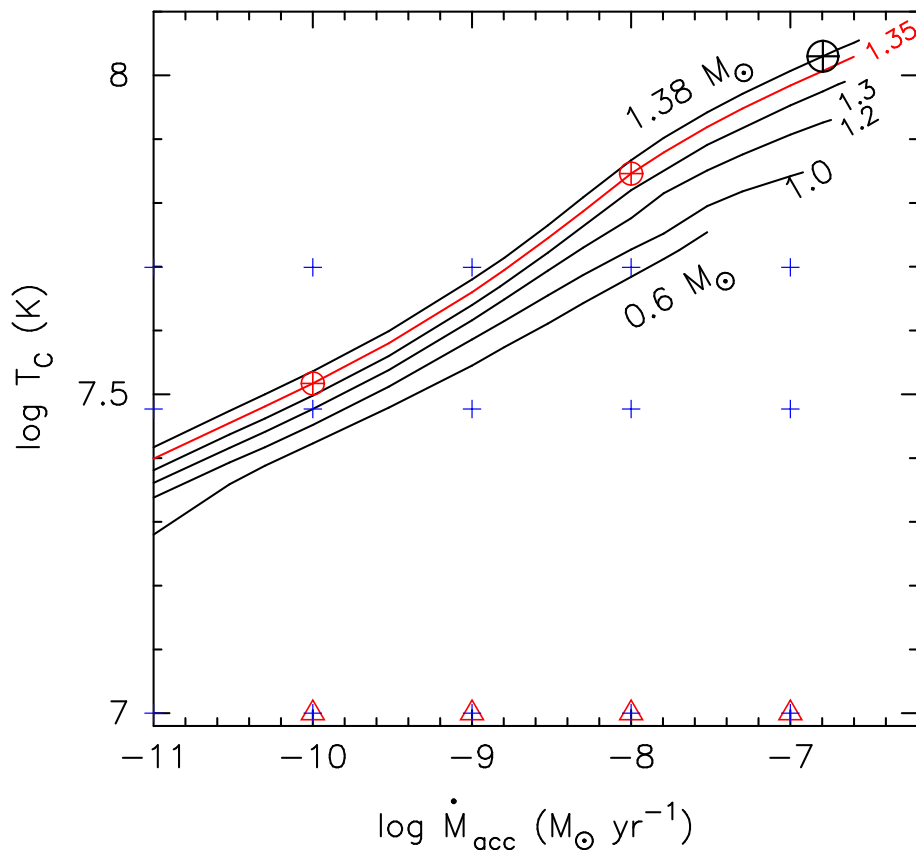
### 3.4 Interior Structures of Accreting 1.35 $M_{\odot}$ WDs

Figure 5 shows the interior structures at the onsets of hydrogen flashes of 1.35  $M_{\odot}$  WDs for three different mass-accretion rates,  $\dot{M}_{\text{acc}} = 1.0 \times 10^{-10} M_{\odot} \text{ yr}^{-1}$ ,  $1.0 \times$

$10^{-8} M_{\odot} \text{ yr}^{-1}$ , and  $5.0 \times 10^{-8} M_{\odot} \text{ yr}^{-1}$ . The structures for the first two accretion rates are at the stages when the nuclear burning luminosity rises to  $5.4 \times 10^3 L_{\odot}$  while the last one is at the slightly later stage when to  $8.0 \times 10^5 L_{\odot}$ .

Figure 5(a) shows distributions of the pressure (black lines) and temperature (red lines). The pressure hardly depends on the mass-accretion rate. The temperature is determined from the energy balance between gravitational energy release and neutrino loss. As shown in the figure, the temperature is almost isothermal throughout the WD interior owing to efficient conductive energy transport. The gravitational energy release rate is larger for higher mass-accretion rates, so the resultant temperature is higher in the larger mass-accretion models.

Figure 5(b) shows the degeneracy,  $\psi$ , i.e., the chemical potential of an electron in units of  $kT$ , where  $k$  is the Boltzmann constant. The degeneracy  $\psi$  takes a large positive value for strongly degenerated matter, and  $\psi \lesssim 0$  for non-degenerated matter. The WD interior is strongly degenerated for the lowest mass-accretion rate



**Fig. 3.** The central temperature  $T_c$  vs. mass accretion rate  $\dot{M}_{\text{acc}}$  of the models in figure 2. From lower to upper, 0.6, 1.0, 1.2, and 1.3  $M_{\odot}$  (black line), 1.35  $M_{\odot}$  (red line), and 1.38  $M_{\odot}$  (black line) WDs. The black encircled plus symbol denotes the central temperature of a 1.38  $M_{\odot}$  WD with  $\dot{M}_{\text{acc}} = 1.6 \times 10^{-7} M_{\odot} \text{ yr}^{-1}$  after it had experienced 10 and 1543 hydrogen shell flashes (two black symbols are overlapped because the central temperature hardly changed). The two red encircled plus symbols indicate the 1.35  $M_{\odot}$  models in Figure 5 with  $\dot{M}_{\text{acc}} = 1 \times 10^{-10}$  and  $1 \times 10^{-8} M_{\odot} \text{ yr}^{-1}$ . The blue cross indicates the assumed core temperature, 1, 3, and  $5 \times 10^7$  K in Prialnik & Kovetz (1995) and Yaron et al. (2019). The open red triangles are in Chen et al. (2019).

( $\dot{M}_{\text{acc}} = 1.0 \times 10^{-10} M_{\odot} \text{ yr}^{-1}$ ) while moderately degenerated in the other two cases.

In the very surface region, the degeneracy is much weaker or almost lifted as shown by the red lines in Figure 5(c)(d)(e). The boundary of the accreted H-rich matter and the CO WD is indicated by the black dot on the radius distribution line.

Figure 5(d) shows the interior structures (dotted lines) at a slightly later stage when the nuclear burning increases to  $L_{\text{nuc}} = 7.8 \times 10^5 L_{\odot}$ . Nuclear energy (heat) flows toward both sides, not only outward but also inward. As a result, the degeneracy and density decrease and the H-rich envelope starts to expand from the place indicated by the black dot.

### 3.5 Summary: Difference Between Classical Novae and Recurrent Novae

A recurrent nova is a nova with multiple recorded outbursts. Its recurrence time is less than a century. From

figure 2, a short recurrence time corresponds to the mass accretion rate of  $\dot{M}_{\text{acc}} \gtrsim 10^{-8} M_{\odot} \text{ yr}^{-1}$  and very massive WDs ( $\gtrsim 1.3 M_{\odot}$ ). On the other hand, many classical novae correspond to relatively less massive WDs with lower mass-accretion rates.

Figures 2, 3, 4, and 5 tell us that even when the WD masses are the same, the difference in the mass-accretion rate causes a substantial difference in the WD internal structure. In recurrent novae, the entire WD is warmed by the large gravitational energy release rate owing to the higher mass-accretion rate. Then the central temperature is relatively high, the WD radius is slightly larger (expanded), the ignition mass is smaller, and the accreted H-rich matter is non-degenerate. Then, the resultant shell flashes are relatively weak.

On the other hand, in classical novae with lower mass-accretion rates, the WD is relatively cooler and has a slightly smaller radius  $R_b$ . The ignition mass is large, and the accreted matter is strongly degenerated. Such a WD will experience a stronger thermonuclear runaway.

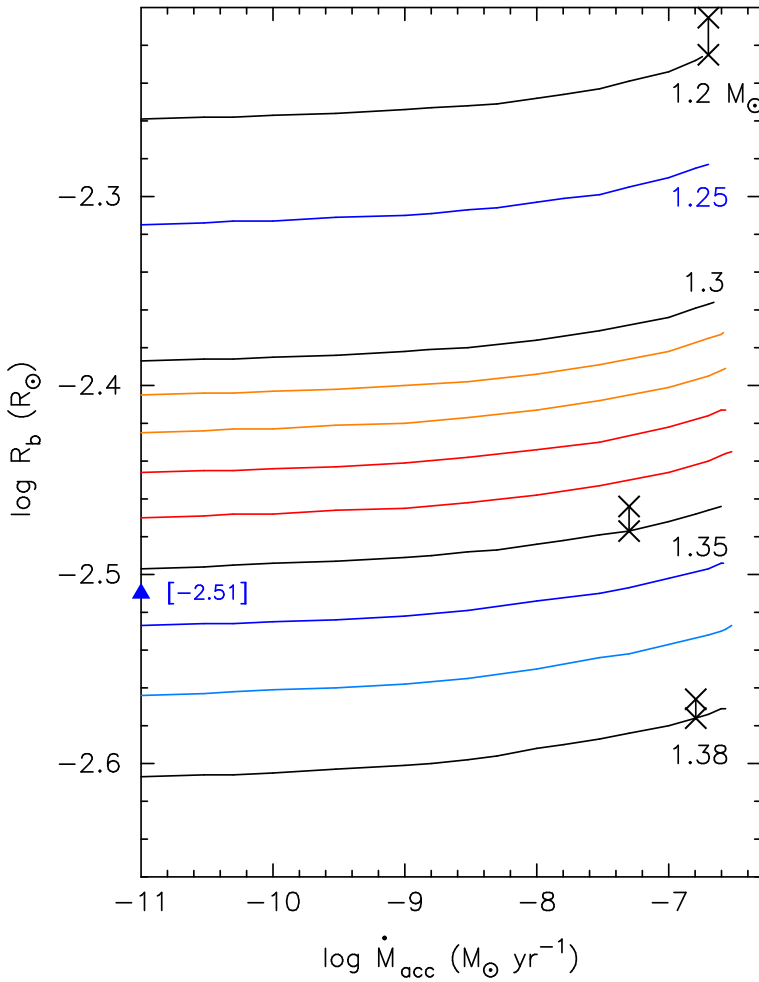


**Fig. 4.** The radius  $R_b$ , where the ignition occurs at the bottom of the H-rich envelope, is shown against the mass accretion rate. From upper to lower, the WD mass is 1.2 (black solid line), 1.25 (blue), 1.3 (black), 1.31 and 1.32 (orange), 1.33 and 1.34 (red), 1.35 (black), 1.36 (blue), 1.37 (sky blue), and 1.38  $M_\odot$  (black). The three pairs of X symbols connected with a line are taken from the models in figure 8. The lower/upper symbol denotes the radius before/after the shell flash. See section 5.1 for more details.

Because the envelope mass at ignition is larger, we expect a brighter optical peak and massive ejecta comparing with those in a recurrent nova having the same WD mass as we see in the next section.

#### 4 Nova Light Curves Based on the Steady-State Approximation

A nova outburst evolution can be followed by a sequence consisting of steady-state envelope solutions with wind mass-loss and without wind mass-loss (static envelope solutions after the winds stop). The wind is accelerated deep interior around the Fe peak in the opacity ( $T \sim 2 \times 10^5$  K) (Kato & Hachisu 1994). We calculated optical light curves of free-free emission that comes from optically thin ejecta near outside the photosphere, which can be approximated as  $F_\nu \propto \dot{M}_{\text{wind}}^2 / (v_{\text{ph}}^2 R_{\text{ph}})$  (Hachisu & Kato 2006). The calculated light curve decays as  $F_\nu \propto t^{-1.75}$  until the bright-

ness drops by about 5 mag from the peak, followed by a steeper decline of  $F_\nu \propto t^{-3.5}$  (Hachisu & Kato 2006). This decline trend is independent of the WD mass and chemical composition of the envelope. Therefore, Hachisu & Kato (2006) called this trend “the universal decline law” of nova light curves.

The optical light curve decays faster in more massive WDs with smaller  $X$  and larger  $Z$ . Such parameter dependences are already discussed in detail in Kato & Hachisu (1994), Hachisu & Kato (2006), Hachisu & Kato (2010), Hachisu & Kato (2015), Hachisu & Kato (2016b), Hachisu & Kato (2018a), Hachisu & Kato (2018b), and Hachisu & Kato (2019b), but the dependence on the WD radius ( $R_b$ ) has not been clarified. In section 3, we see that the WD radius depends on the mass accretion rate even if the WD masses are the same; The radius is smaller (larger) for a lower (higher) mass accretion rate. Here we discuss the dependence of the light curve on the WD radius for a



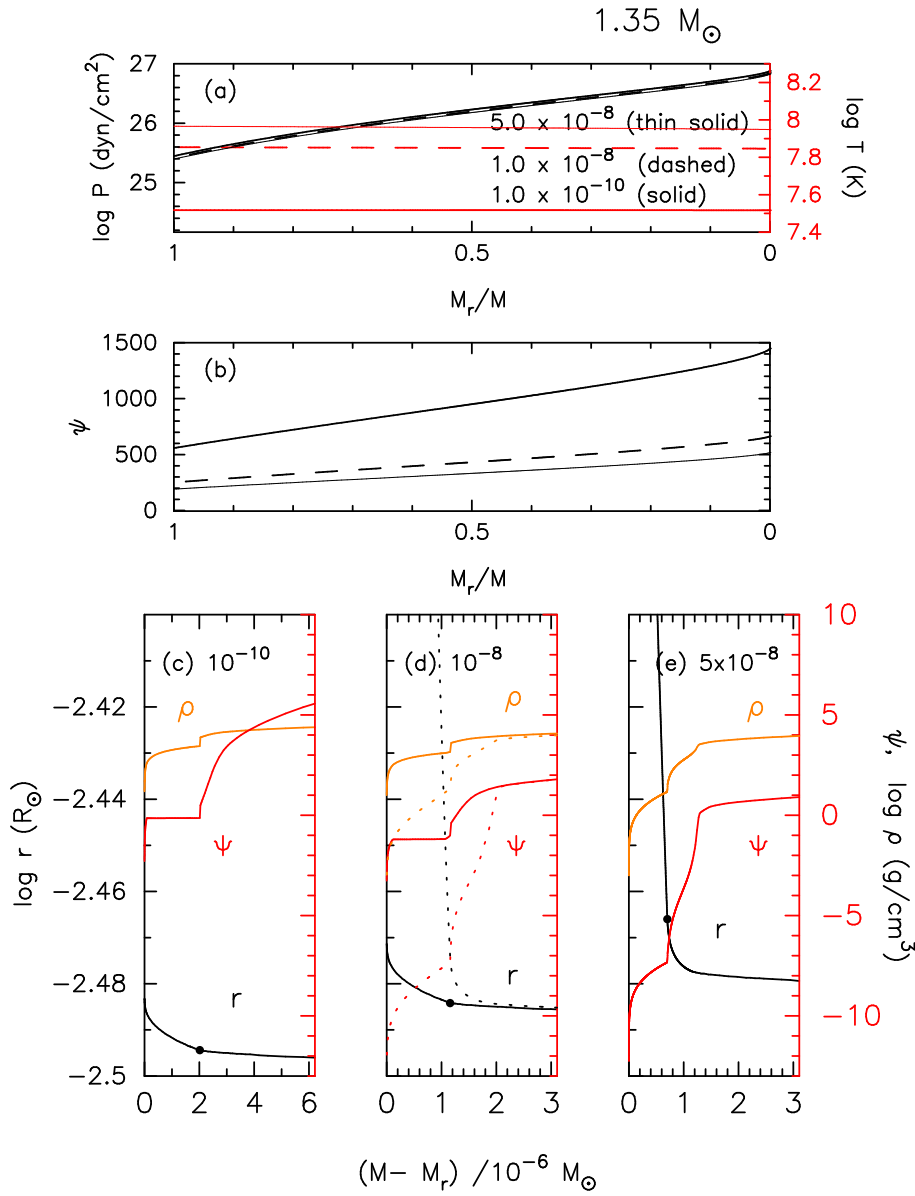


**Fig. 5.** Various interior structures of mass-accreting  $1.35 M_{\odot}$  WDs. (a) The distributions of the pressure  $P$  (black lines) and temperature  $T$  (red lines) against the mass coordinate  $M_r/M$ , where  $M_r$  is the mass within the radius  $r$  and  $M$  is the total mass of the WD. (b) The degeneracy  $\psi$  from the WD center (the right edge) to the surface (the left edge). In panels (a) and (b), the accretion rate is  $\dot{M} = 1 \times 10^{-10} M_{\odot} \text{ yr}^{-1}$  (thick solid line),  $\dot{M} = 1 \times 10^{-8} M_{\odot} \text{ yr}^{-1}$  (dashed line), and  $\dot{M} = 5 \times 10^{-8} M_{\odot} \text{ yr}^{-1}$  (thin solid line). (c)(d)(e) The bottom three panels show the degeneracy  $\psi$  (red), radius  $r$  (black), and density  $\rho$  (orange) against  $(M - M_r) / 10^{-6} M_{\odot}$ , i.e., in the very surface layer for the three different mass accretion rates,  $1 \times 10^{-10}$ ,  $1 \times 10^{-8}$ , and  $5 \times 10^{-8} M_{\odot} \text{ yr}^{-1}$ , respectively. The left edge of each figure corresponds to the surface of accreted H-rich envelope, the bottom of which is indicated by the black dot on the  $r$  distribution. See the main text for other details.

1.35  $M_{\odot}$  WD.

#### 4.1 1.35 $M_{\odot}$ WD Models for Different Parameters

Figure 6(a) compares light curves of 1.35  $M_{\odot}$  WDs having various WD radii  $R_b$ . The chemical composition is assumed to be Ne nova 2 (25 % mixing) from a grid chemical composition model (Hachisu & Kato 2010), which seems to be close to the chemical composition obtained for V2491 Cyg by Munari et al. (2011), i.e.,  $X = 0.573$ ,  $Y = 0.287$ , and  $Z = 0.140$ . The three X-ray light curves, which are closely located, are the models with the radius, from left to right,  $\log R_b/R_{\odot} = -2.492$  (red line),  $-2.479$  (black), and  $-2.468$  (blue). These radii correspond to the one at ignition of a cold WD with  $\dot{M}_{\text{acc}} = 5 \times 10^{-10} M_{\odot} \text{ yr}^{-1}$ , an expanded radius after the ignition, and the radius at ignition for  $\dot{M}_{\text{acc}} = 5 \times 10^{-8} M_{\odot} \text{ yr}^{-1}$ , respectively.

The three optical light curves (come from free-free emission) are very similar except in the later phase ( $t \gtrsim 30$  d). The free-free light curve is mainly determined by the wind mass-loss rate  $\dot{M}_{\text{wind}}$ . The wind is accelerated in the Fe peak region of OPAL opacity ( $T \sim 1.5 \times 10^5$  K), which is located far outside the nuclear burning region ( $T \sim 10^8$  K). Thus, the wind mass-loss rate is not sensitive to the WD radius. In the later phase, the wind mass-loss rate decreases and becomes comparable to the mass decreasing rate due to nuclear burning. The nuclear burning rate is sensitive to the WD radius. For a smaller radius, the burning temperature is higher, so the nuclear burning rate is larger. Thus, the light curve decays faster for a smaller WD radius.

The X-ray flux quickly rises when the wind mass-loss stops (at  $t \sim 40$  d) and decays after  $\sim 10$  days. This X-ray turn on time ( $t_{\text{on}} \sim 40$  d) and the short SSS duration ( $\Delta t_{\text{SSS}} \sim 10$  d) are very consistent with the observed X-ray turn-on time of V2491 Cyg and its duration. In the next subsection, we will make a composite light curve model of V2491 Cyg.

For comparison, we add a light curve model corresponding to a recurrent nova with the same WD mass (1.35  $M_{\odot}$ ) but with a different chemical composition taken from the model in section 5 (figure 8(b)),  $X = 0.55$ ,  $Y = 0.43$ , and  $Z = 0.02$ . This model shows much slower evolution because the wind acceleration is relatively weak due to the difference in the opacity. When the wind mass-loss stops, the envelope mass is larger by a factor of 1.6 compared with those in classical nova models. This makes the SSS duration longer than the classical nova models.

Figure 6(b) shows three WD models of different masses but with the same recurrent nova composition. The magenta line (1.35  $M_{\odot}$ ) model is the same as in the upper

panel. In a more massive WD, the optical light curve decays faster and the SSS phase is shorter. The 1.38  $M_{\odot}$  model shows an earlier X-ray turn-on time and shorter SSS duration, roughly consistent with the characteristic properties of V2491 Cyg. However, this model is based on the composition of  $X = 0.55$ ,  $Y = 0.43$ , and  $Z = 0.02$ , being inconsistent with the estimates of heavy element enrichment (Munari et al. 2011). Thus, we reject the recurrent nova model for V2491 Cyg.

The X-ray turnoff time ( $t \sim 90$  d) of the 1.35  $M_{\odot}$  model with the recurrent nova composition is roughly consistent with the recurrent nova RS Oph. However, the model X-ray flux rises much later and hence the model SSS phase is much shorter than the observed one. Hachisu et al. (2007) already reported this discrepancy in the steady-state model calculated for RS Oph. Here, we add another inconsistency between the envelope mass and ignition mass. In the optical light curve shown in figure 6(b), the envelope mass is  $M_{\text{env}} = 5 \times 10^{-6} M_{\odot}$  at the peak of the dotted part of the 1.35  $M_{\odot}$  model. This is much larger than the expected ignition mass for a recurrent nova,  $M_{\text{ig}} = 7 \times 10^{-7} M_{\odot}$  at  $\dot{M}_{\text{acc}} = 5 \times 10^{-8} M_{\odot} \text{ yr}^{-1}$  as shown in figure 2. If we adopt the small ignition mass ( $M_{\text{env}} = M_{\text{ig}} = 7 \times 10^{-7} M_{\odot}$ ), the optical light curve would start from the top of the solid part rather than the dotted part, which is much fainter as a recurrent nova.

To summarize, the steady-state model reproduces a consistent light curve for V2491 Cyg as a classical nova, but do not for the recurrent nova RS Oph. In section 5, we discuss the reason why the steady-state approximation fails to reproduce recurrent novae.

#### 4.2 V2491 Cyg Model

We have calculated a light curve model for V2491 Cyg, assuming that the WD mass is 1.36  $M_{\odot}$ , its radius is  $\log(R_b/R_{\odot}) = -2.51$ , and the envelope chemical composition is Ne nova 2. The radius  $R_b$  is indicated by the filled blue triangle at  $\dot{M}_{\text{acc}} = 1 \times 10^{-11} M_{\odot} \text{ yr}^{-1}$  in figure 4. This mass-accretion rate is obtained assuming that the envelope mass at the optical peak, which is calculated later in the light curve fitting for V2491 Cyg, is the same as that of the ignition mass (Hachisu et al. 2020). Figure 7 shows our light curve model. The optical free-free emission light curve is fitted to the observational data assuming  $(m - M)_V = 16.65$  (Hachisu & Kato 2021). The X-ray luminosity calculated with the blackbody assumption is arbitrarily shifted in the vertical direction to fit the observed X-ray count rates.

The theoretical light curve decays as  $F_{\nu} \propto t^{-1.75}$ , and fits the observational data only in the very early phase

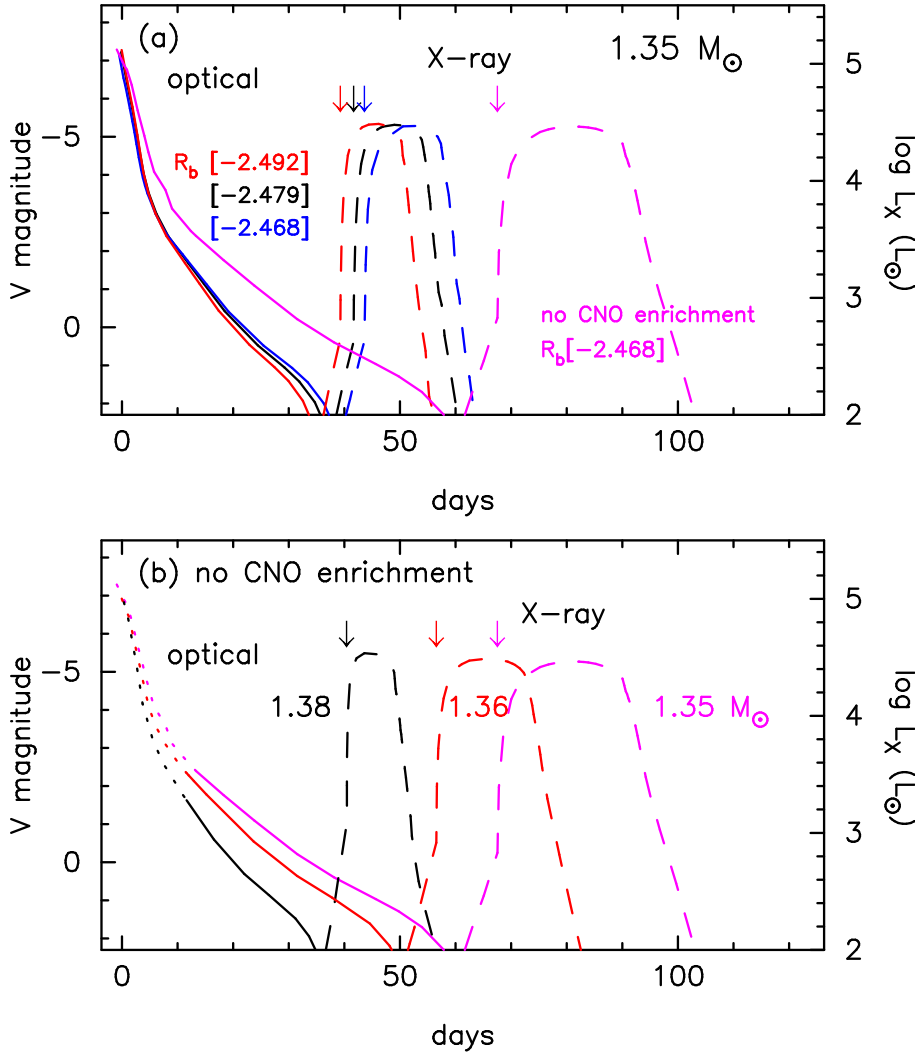


**Fig. 6.** Theoretical light curve models of optical free-free emission (solid lines) and X-ray blackbody emission (dashed lines) based on the steady-state assumption. (a) Comparison of theoretical light curves for  $1.35 M_{\odot}$  WDs with three different radii of  $\log(R_b/R_{\odot}) = -2.492$  (very cold WD: red),  $-2.479$  (black), and  $-2.468$  (blue). The chemical composition of the envelope is assumed to be Ne nova 2 ( $X = 0.55$ ,  $Y = 0.3$ ,  $X_{\text{CNO}} = 0.10$ ,  $X_{\text{Ne}} = 0.03$ ,  $Z = 0.02$  by mass fraction). For comparison we added the magenta lines of  $X = 0.55$ ,  $Y = 0.43$  and  $Z = 0.02$  with a radius of  $\log(R_b/R_{\odot}) = -2.468$  that may represent a case of recurrent nova like RS Oph. The downward arrow indicates the epoch when the optically thick wind stops in each model. (b) Comparison of the light curves for different WD masses but with the same recurrent nova composition ( $X = 0.55$ ,  $Y = 0.43$ ,  $Z = 0.02$ ). In the dotted part of the optical light curve, the envelope mass exceeds the ignition mass for  $\dot{M}_{\text{acc}} = 3 \times 10^{-8} M_{\odot} \text{ yr}^{-1}$ . See the main text for more detail.

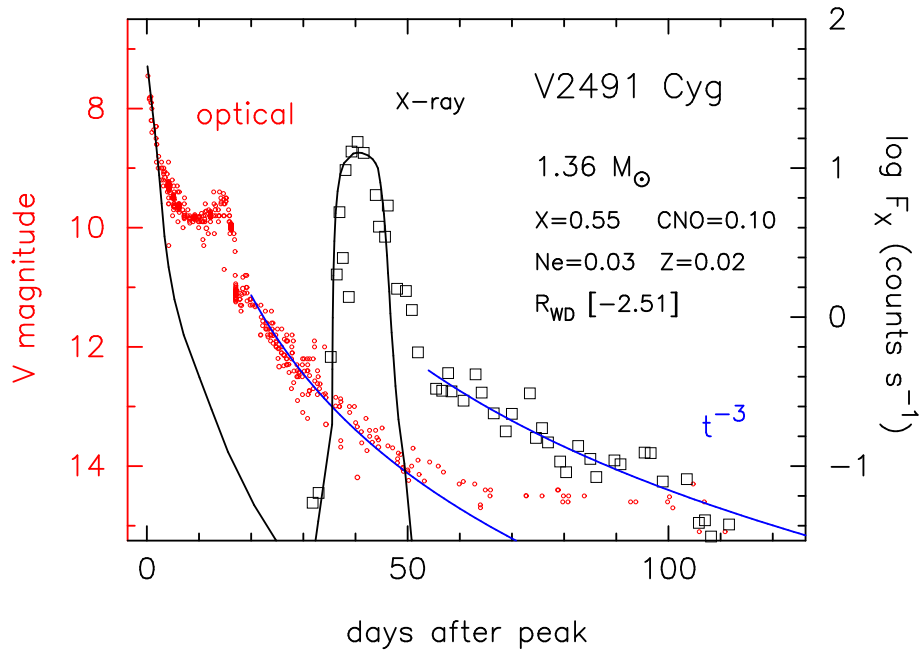


**Fig. 7.** A model light curve fitting for V2491 Cyg. The thick black line indicates the optical (free-free emission) and X-ray (blackbody) light curves for a  $1.36 M_{\odot}$  WD with the radius of  $\log(R_b/R_{\odot}) = -2.51$ . The envelope chemical composition is Ne nova 2. The thin blue lines indicate the  $F_{\nu} \propto t^{-3}$  law that represents free-free emission from freely expanding plasma with a constant mass, ejected on Day 0.

down to  $V \sim 9$ . Such a rapid decay is due to the massive WD and heavy element enrichment as shown in the previous subsection. The calculated wind mass-loss rate is largest at the optical peak,  $\dot{M}_{\text{wind}} = 3.6 \times 10^{-4} M_{\odot} \text{ yr}^{-1}$ , and quickly decreases with time until the wind stops at  $t = 35.7$  d. This quick decrease of the wind mass-loss rate is the reason for the steep decline of the optical light curve.

Here we do not consider the second peak at Day  $\sim 15$ , which can be explained by some additional mechanism like the magnetic energy release (Hachisu & Kato 2009). After the second peak, the theoretical curve is much fainter than the observed one. From our experience of a number of light curve fittings, nova brightnesses sometimes show much excess than the theoretical one of  $F_{\nu} \propto t^{-1.75}$ . One of the reasons is shock heating. Hachisu & Kato (2018b) examined light curves of fast novae and recurrent novae and showed that shock heating makes the light curve decay slower than  $F_{\nu} \propto t^{-1.75}$ . For example, in the symbiotic classical nova V407 Cyg, the V magnitude decays as  $F_V \propto t^{-1}$  until the shock breakout. In RS Oph, the Solar Mass Ejection Imager (SMEI) magnitude decays as  $F_{\text{SMEI}} \propto t^{-1}$ , while the V magnitude decays as  $F_V \propto t^{-1.55}$ . The other effect is nebular line emission. In many classical novae observed data follow the theoretical line but becomes much brighter in V magnitude when they enter the nebular phase. It is because the ejecta are ionized by high energy radiation from the hot WD and many emission lines contribute to the V magnitude. Typically the light curve roughly de-

cays as  $F_{\nu} \propto t^{-3}$  in the nebular phase (e.g. V1974 Cyg in Woodward et al. (1997); LV Vul in figure 24, V1500 Cyg in figure 45, both of Hachisu & Kato (2019b)).

In the case of V2491 Cyg, it is unlikely that the companion is a red giant, and therefore we do not expect cool red-giant winds, as discussed in section 2. Instead, we expect that massive ejecta could contribute to the optical V magnitude. In the model in figure 7, the envelope mass at the optical peak ( $t = 0$  d) is  $M_{\text{env}} = 2.4 \times 10^{-6} M_{\odot}$ , which is quickly reduced by the wind mass-loss to  $M_{\text{env}} = 3.3 \times 10^{-7} M_{\odot}$  until  $t = 10.3$  d, the beginning of the second peak, and to  $M_{\text{env}} = 7.4 \times 10^{-8} M_{\odot}$  at  $t = 35.7$  d when the optically thick winds stopped. Thus, 90% of the envelope mass is ejected until the second peak. If we approximate the ejecta mass to be constant after the second peak, the V brightness decays approximately along the line of  $F_V \propto t^{-3}$  in figure 7. The decline rate of  $t^{-3}$  represents emission from optically thin plasma, the mass of which is constant in time, but expands freely (see, e.g., equation (1) of Woodward et al. (1997)). The model line of  $F_V \propto t^{-3}$  shows a good agreement with the observed V magnitudes. The photospheric temperature of the WD rises from  $\log T$  (K)=4.00 at  $t = 0$  d, to 4.95 at  $t = 10.3$  d, and 5.54 at  $t = 35.7$  d.

The supersoft X-ray flux (0.3 - 1.0 keV) is calculated from the blackbody emission at the WD photosphere. The predicted X-ray right curve quickly rises just after the wind stops at Day 35.7. After staying on the maximum level for

$\sim 10$  days, it decays quickly at Day  $\sim 50$  when nuclear burning is extinguished. On the other hand, the observed flux decays slowly after Day 50. To explain this slow decay we added another line of  $t^{-3}$ . The model line of  $F_X \propto t^{-3}$  shows a good fit with the X-ray count rates after the SSS phase. The ejecta is heated by the WD and emit X-rays by thermal Bremsstrahlung process (free-free emission). This is essentially the same as the process in the optical  $V$  band.

The envelope mass at the optical peak  $M_{\text{env}} = 2.1 \times 10^{-6} M_{\odot}$  is consistent with the ignition mass at the mass accretion rate of  $\log \dot{M}_{\text{acc}} (M_{\odot} \text{ yr}^{-1}) = -11$  for  $1.36 M_{\odot}$  ( $M_{\text{ig}} = 2.0 \times 10^{-6} M_{\odot}$ ) in figure 2. This ignition mass is marked with the filled triangle in figure 2. This low mass-accretion rate is consistent with a theory of Maximum Magnitude vs. Rate of Decline (MMRD) (Hachisu et al. 2020) as mentioned in section 2 and our assumption of a cooler WD having a smaller  $R_b$ . In this way, our classical nova model consistently explains the optical and X-ray light curves of V2491 Cyg.

## 5 Comparison with Evolution Models

In the previous section, we see that the steady-state model explains the optical and X-ray light curves of V2491 Cyg. A good way to evaluate the steady-state approximation is to compare their internal structure with evolution models. However, no internal structures have been published in evolution code calculations for classical novae after the opacity tables are revised in 1990's (see Kato et al. (2017c) for more details). Therefore, we concentrate on recurrent novae and compare our Henyey-type code solutions with steady-state solutions to see the reason why the light curve of RS Oph is different from that of V2491 Cyg.

### 5.1 Three Recurrent Nova Models

Figure 8 shows our time-dependent models of a  $1.2 M_{\odot}$  WD with  $\dot{M}_{\text{acc}} = 2 \times 10^{-7} M_{\odot} \text{ yr}^{-1}$  ( $P_{\text{rec}} = 9.9 \text{ yr}$ ),  $1.35 M_{\odot}$  WD with  $\dot{M}_{\text{acc}} = 5 \times 10^{-8} M_{\odot} \text{ yr}^{-1}$  ( $P_{\text{rec}} = 12 \text{ yr}$ ), and  $1.38 M_{\odot}$  WD with  $\dot{M}_{\text{acc}} = 1.6 \times 10^{-7} M_{\odot} \text{ yr}^{-1}$  ( $P_{\text{rec}} = 0.95 \text{ yr}$ ). The calculation method and the results for the  $1.2 M_{\odot}$  and  $1.38 M_{\odot}$  models are already published in Kato et al. (2017a). The left column in figure 8 shows the last cycles of each sequence, and the middle column shows the close-up view of the last flash, i.e., the change of the photospheric luminosity  $L_{\text{ph}}$ , total nuclear burning rate  $L_{\text{nuc}}$ , and gravitational energy release rate  $L_G$ . The exact definition of  $L_{\text{nuc}}$  and  $L_G$  are given in Hachisu et al. (2016). During the early outburst, a large amount of nuclear energy  $L_{\text{nuc}}$  ( $> 10^6 L_{\odot}$ ) is generated, much larger than the Eddington luminosity  $L_{\text{Edd}} = 4\pi cGM/\kappa$ . Most of the energy is ab-

sorbed but a part of it flows outward to the photosphere. As a result, the photospheric luminosity  $L_{\text{ph}}$  does not exceed but is almost equal to the Eddington luminosity. This absorbed energy flux, expressed as a negative value of  $L_G$ , is released shortly later, and  $L_G$  turns to be positive.

The rightmost panels show the change of the radius at the bottom of hydrogen nuclear burning region  $R_b$ . The radius  $R_b$  quickly rises at the onset of thermonuclear runaway because the envelope is heated and expanded, resulting in the decrease of pressure at  $R_b$ . The radius keeps almost constant with gradual decrease in the temperature, followed by quick decrease when  $L_{\text{nuc}}$  drops quickly. We indicate the degeneracy at the center of the WD,  $\psi_c$ , as a representative value of thermal condition for the WD interior as shown in figure 5(b). The logarithmic radius increase  $\Delta \log R_b$  is larger for a smaller central degeneracy  $\psi_c$ , because weakly degenerated matter is easily expanded than in the tightly degenerated case (A shell flash occurs even if the envelope is not degenerated. See discussion in section 6.2).

### 5.2 Envelope Structure

Figure 9 shows the distribution of  $r$ ,  $T$ ,  $L_r$ ,  $L_{\text{nuc}}$ , and  $L_G$  against the density at the epoch when the wind mass loss stops as indicated by the dot in figure 8. The rightmost point is the center of the WD. Hydrogen nuclear burning occurs at  $\log \rho (\text{g cm}^{-3}) = 1 - 2$ , where the nuclear luminosity  $L_{\text{nuc}}$  quickly increases outward (leftward). Convection does not occur in this stage. Heat flows not only outward but also inward. As a result, the temperature distribution has a temporal flat peak at  $\log \rho (\text{g cm}^{-3}) = 1.5 - 3$ , that disappears until the end of the shell flash. In the inner region to the temporal peak, the temperature profile hardly changes with time, regardless the phase of the shell flash. The temperature slightly decreases at the center of the WD because of neutrino energy loss.

The gravitational energy release represents non-homologous (local) response of the envelope to heat generation/transport. It takes negative values when the envelope absorbs energy to expand while positive when loses energy to shrink. The integrated gravitational energy release rate,  $L_G$ , increases outward in the region  $\log \rho (\text{g cm}^{-3}) = -2 - +2$  and becomes constant outside this density region. This means that the inner part of the envelope is locally shrinking to release gravitational energy. This  $L_G$  term can be calculated only in the evolution code and is not included in hydrostatic steady-state solutions. Thus, the amount of  $L_G$  is a measure of the deviation from hydrostatic steady-state structure.

The radiative luminosity is the summation of the nu-

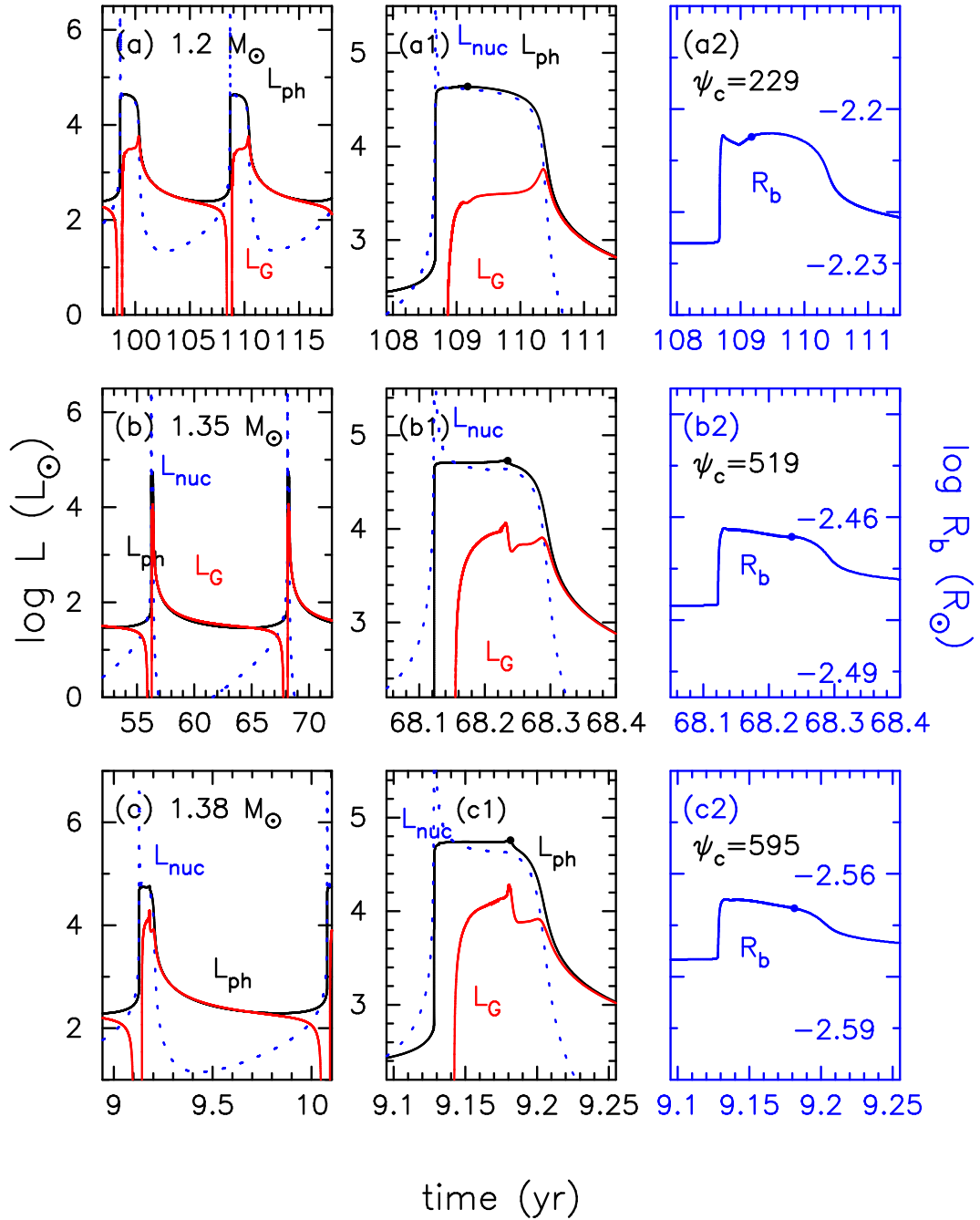


**Fig. 8.** Evolution models of (a) 1.2  $M_{\odot}$  WD with  $\dot{M}_{\text{acc}} = 2 \times 10^{-7} M_{\odot} \text{ yr}^{-1}$ , (b) 1.35  $M_{\odot}$  WD with  $\dot{M}_{\text{acc}} = 5 \times 10^{-8} M_{\odot} \text{ yr}^{-1}$ , and (c) 1.38  $M_{\odot}$  WD with  $\dot{M}_{\text{acc}} = 1.6 \times 10^{-7} M_{\odot} \text{ yr}^{-1}$ . The left column shows the temporal changes of the photospheric luminosity  $L_{\text{ph}}$  (black line), gravitational energy release rate  $L_{\text{G}}$  (red line), and nuclear burning rate  $L_{\text{nuc}}$  (dotted blue line) of the last two cycles of our calculation. The black dot represents the stage when the wind mass-loss stops, i.e., the beginning of the SSS phase. The right column shows the radius of the bottom of nuclear burning region, the scale of which is indicated inside of the figure. The degeneracy at the center of the WD,  $\psi_{\text{c}}$ , is also indicated.

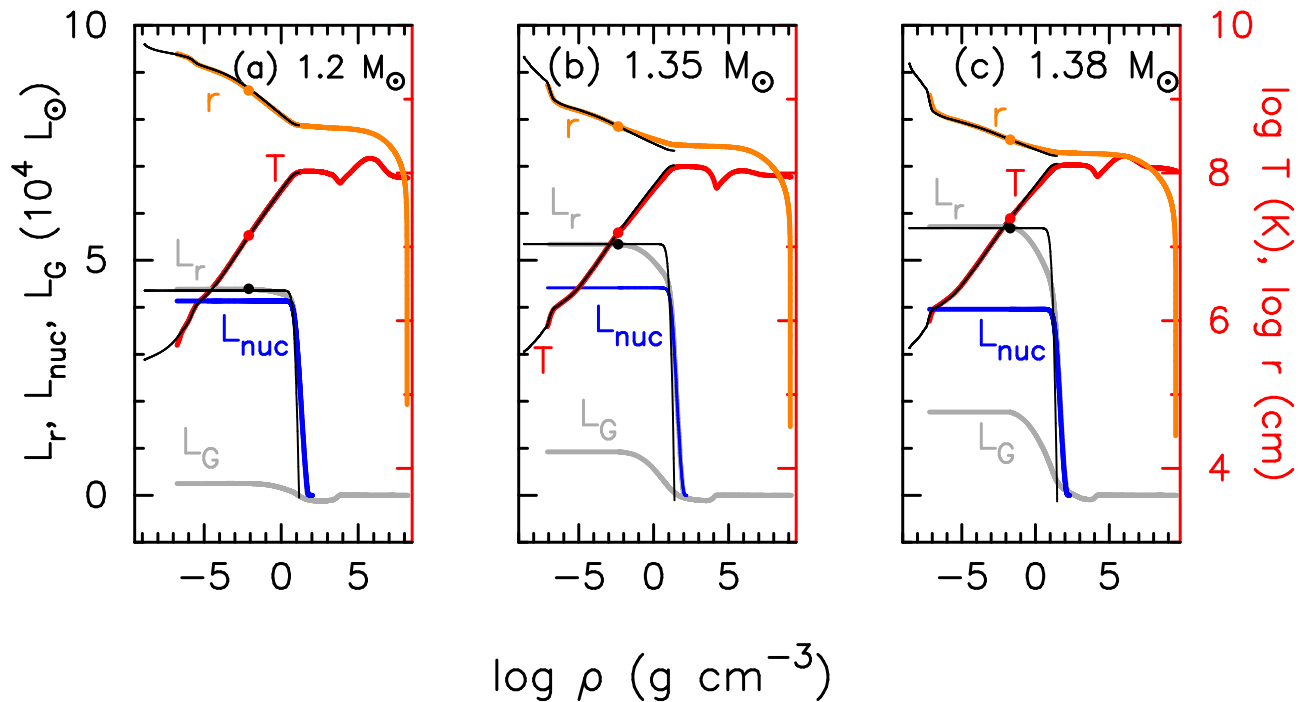


**Fig. 9.** Internal structures of the WDs obtained with our Henyey code, (a)  $1.2 M_{\odot}$  WD, (b)  $1.35 M_{\odot}$  WD, and (c)  $1.38 M_{\odot}$  WD models at the epoch when the wind mass loss just stops, which are indicated by the dot in figure 8. The radius  $r$ , temperature  $T$ , radiative flux  $L_r$ , integrated nuclear burning rate  $L_{\text{nuc}}$ , and integrated gravitational energy release rate  $L_G$  are plotted against the density. We omit the inner part of the  $L_{\text{nuc}}$  line, where it becomes zero, to clarify the negative value of  $L_G$ . The thin black lines represent those of the hydrostatic solution of steady-state approximation. The matching point with the Henyey code solution is indicated by the dot. See the main text for more details.

clear luminosity and gravitational energy release rate,  $L_r = L_{\text{nuc}} + L_G$ , because neutrino loss is very small. For the three cases in figure 9,  $L_G$  is larger in more massive WDs and as large as about a half of  $L_{\text{nuc}}$  in the  $1.38 M_{\odot}$  WD. Note, however, that  $L_G$  takes the maximum value at this epoch in  $1.35 M_{\odot}$  and  $1.38 M_{\odot}$  WDs (see figure 8) and decreases after that.

### 5.3 Comparison with Hydrostatic Solutions of Steady-state Approximation

Figure 9 compares the internal structures of evolution models calculated with a Henyey code (thick solid lines) with hydrostatic steady-state solutions (thin solid black lines). The two solutions are fitted at the matching point (the filled circles) to have the same temperature, radius and luminosity  $L_r$  (See Kato et al. (2017a) for more details).

In the  $1.2 M_{\odot}$  WD, the temperature  $T$  and radius  $r$  of these two different solutions are very close to each other not only in the outside region to the matching point but also inside region down to the place where  $L_{\text{nuc}} = 0$ . In the  $1.35 M_{\odot}$  and  $1.38 M_{\odot}$  WDs, the hydrostatic steady-state solution fits well with the evolution solution in the  $r$ ,  $T$ , and  $L_r$  distributions in the outside region to the fitting

point. Although the hydrostatic steady-state solutions do not include  $L_G$ , we obtain a rather good agreement with the  $L_r = L_{\text{nuc}} + L_G$  evolution solutions. In other words, the static steady-state solution is close to those of evolution solution even when  $L_G$  substantially contributes to the total luminosity as far as  $L_r$  is constant outside the fitting point.

In the time-dependent solution,  $L_G$  decreases inward differently from  $L_{\text{nuc}}$ . This causes the large deviation in the  $L_r$  distribution, and also in the envelope mass distribution. Thus, the evolution time is different between evolution calculation and steady-state wind and hydrostatic sequence. We may say that steady-state wind/hydrostatic treatment is a good approximation when  $L_G$  is small compared with  $L_r$  because the envelope structure is close to that of evolution solution, but not always good when  $L_G$  is comparable to  $L_r$ . We will discuss this point in section 6.1.

## 6 DISCUSSION

### 6.1 Steady-State Approximation

We calculated the light curve model with steady-state approximation in section 4.2. This model explains the ob-

served light curves of the classical nova V2491 Cyg. On the other hand, the model light curves for the recurrent nova composition (magenta line in figure 6) does not fit to the X-ray light curve of RS Oph. These two novae host similar WD masses ( $\sim 1.35 - 1.36 M_{\odot}$ ), but with very different mass-accretion rates. Here, we discuss the reason why the steady-state assumption is good for classical novae (with lower mass-accretion rates), but not for recurrent novae (with higher mass-accretion rates), even with similar WD masses.

Kato's (1983, 1985) optically thick wind theory is to follow a nova outburst with a sequence of steady-state wind and static solutions (see also Kato & Hachisu (1994) for OPAL opacity). The time between two consecutive solutions is calculated from the difference in the envelope mass and its decreasing rate due both to wind mass-loss and nuclear burning. After the wind stops, the envelope mass decreases only with nuclear burning.

In the SSS phase, we calculate the envelope mass-decreasing rate based on the nuclear luminosity,  $L_{\text{nuc}} = L_{\text{ph}}$ . We would overestimate the mass-decreasing rate when  $L_{\text{G}}$  substantially contributes to the total luminosity, i.e.,  $L_{\text{nuc}} < L_{\text{ph}}$ . Thus, the SSS phase could be shorter than the evolution calculation, as expected from figure 8(a)(b)(c).

When strong optically-thick winds occur in the early phase of a nova outburst, the timescale is determined mainly by the wind mass-loss rate because the total mass decreasing rate is determined mainly by the wind mass-loss rate not by the nuclear burning rate. Thus, the effect of  $L_{\text{G}}$  on the timescale is negligible even if  $L_{\text{G}}$  substantially contributes to the total luminosity.

In high mass-accretion rates, the contribution of  $L_{\text{G}}$  is not negligible as already shown in figure 8(a)(b)(c). If its contribution is very small or negligible in low mass-accretion rates, we may conclude that the steady-state approximation is good for classical novae. In order to check this question, we searched literature for hydrogen shell flashes having the description on the contribution of  $L_{\text{G}}$  to the interior structures. Many shell flash calculations have been published so far, but most of them are lack of information on  $L_{\text{G}}$ . Among them, Iben (1982) described energy balance in the WD core between the energy gain owing to gravitational heating and nuclear burning and energy loss by neutrino. In the case of  $1.01 M_{\odot}$  WD with  $\dot{M}_{\text{acc}} = 1.5 \times 10^{-8} M_{\odot} \text{ yr}^{-1}$ , the gravitational heating is as small as  $L_{\text{G}}/L_{\text{nuc}} < 10^{-4}$ . For the case of  $1.5 \times 10^{-9} M_{\odot} \text{ yr}^{-1}$ ,  $L_{\text{G}}$  is not plotted but the photospheric luminosity  $L_{\text{ph}}$  is equal to  $L_{\text{nuc}}$  within the line width in the figure. Thus  $L_{\text{G}} = L_{\text{ph}} - L_{\text{nuc}}$  should be very small. These WD mass and mass accretion rates are typical for classical novae, and we regard that the steady-state approximation

is good.

The above calculation is done before the opacity tables are recalculated in the beginning of 1990's. With the OPAL opacity (Iglesias & Rogers 1996), strong winds are accelerated in the region of  $T \sim 10^5$  K. This region is much outside of the nuclear burning region ( $T \sim 10^8$  K) (see e.g., Kato & Hachisu (1994)). Thus, the opacity does not much affect the deep inside where  $L_{\text{G}}$  is mainly generated. We may conclude that  $L_{\text{G}}$  is also small in shell flash calculation even with the OPAL opacity.

To summarize, the gravitational energy release rate  $L_{\text{G}}$  is very small or negligible in low mass-accretion rates while this effect on the timescale should not be neglected in the SSS phase of high mass-accretion rates. Thus, we may conclude that the steady-state assumption is a good approximation for the classical nova V2491 Cyg.

## 6.2 Shell Flashes in Non-degenerate Envelope

A hydrogen shell flash could occur regardless whether the envelope matter is degenerate or not. Figure 5 shows that the envelope is non-degenerate for high mass-accretion rates. José et al. (1993) presented the shell flash calculation with two-zone approximation in which the temperature in the quiescent phase is as high as  $T = 3.4 \times 10^7$  K ( $\log \rho$  ( $\text{g cm}^{-3}$ )  $\sim 1.8$ ). In the model of a  $1.2 M_{\odot}$  WD with  $\dot{M}_{\text{acc}} = 2 \times 10^{-7} M_{\odot} \text{ yr}^{-1}$ , the bottom of the H-rich envelope is non-degenerate throughout a full cycle of the shell flash.

Sugimoto & Fujimoto (1978) discussed that the most essential factor of thermonuclear runaway is the plane parallel configuration of the envelope structure. When a shell flash begins, nuclear burning produces thermal energy, and both the temperature and pressure at the nuclear burning region increase. This causes a shell expansion. If the envelope structure is spherical, the expansion of the shell results in the pressure decrease. Then, the temperature also decreases. Thus, the nuclear burning is stabilized and runaway does not occur. In the plane parallel configuration, however, the pressure at the bottom of the envelope is written as  $P_{\text{b}} = GM_{\text{WD}} M_{\text{env}} / (4\pi R_{\text{b}}^4)$ , i.e., the pressure is determined only by the envelope mass  $M_{\text{env}}$  and independent of the temperature. When a shell flash occurs keeping the plane parallel structure, the bottom pressure hardly changes, so that the temperature would increase and accelerate nuclear reactions. This causes the thermonuclear runaway. If the matter is strongly degenerate, the pressure is independent of the temperature. The strong degeneracy enhances and accelerates the nuclear burning, but not the necessary condition for shell flashes. The most essential factor for the thermonuclear runaway is the plane parallel



configuration.

### 6.3 WD Core Temperature

In a long-term evolution of an accreting WD, its interior approaches a thermally relaxed state in which the energy gain owing to gravitational contraction of the core and time-averaged nuclear burning balances with the energy loss by neutrino. Iben (1982) obtained such a core temperature of a WD with double shell burning. His accreting WD core is in a thermal balance in which “the release of gravitational potential energy within the core is balanced to go into neutrinos and into rising kinetic energy of electrons and nuclei in the core.” The equilibrium core temperature is obtained to be  $\log T_c$  (K) = 7.84 ( $1.01 M_\odot$ ), 7.90 ( $1.20 M_\odot$ ), and 8.06 ( $1.40 M_\odot$ ) for  $\dot{M}_{\text{acc}} = 1.5 \times 10^{-8} M_\odot \text{ yr}^{-1}$ . We have calculated a similar case using the same method and numerical code in the present work and obtained the WD core temperature to be  $\log T_c$  (K) = 7.87 ( $1.1 M_\odot$ ), 7.88 ( $1.20 M_\odot$ ), and 7.96 ( $1.38 M_\odot$ ) for  $\dot{M}_{\text{acc}} = 2.0 \times 10^{-8} M_\odot \text{ yr}^{-1}$ . These temperatures are in reasonable agreement with Iben’s results. As the burning temperature of helium is much higher than that of hydrogen, these core temperatures are higher than the values in figure 3.

Townsley & Bildsten (2004) calculated the equilibrium core temperature of classical novae, as a function of the accretion rate and accreted mass for a specified WD mass. For example, starting from a  $0.6 M_\odot$  WD with  $\dot{M}_{\text{acc}} = 4 \times 10^{-11} M_\odot \text{ yr}^{-1}$ , they obtained  $T_c = 1.5 \times 10^7$  K for the accreted mass  $1 \times 10^{-4} M_\odot$ . This value is much lower than our results of  $T_c = 2.36 \times 10^7$  K and  $M_{\text{ig}} = 2.57 \times 10^{-4} M_\odot$  for the same WD mass and mass accretion rate. We do not clarify the reason, but this difference probably comes from the approximations adopted in their calculation.

Piersanti et al. (2000) calculated hydrogen shell flashes for a  $0.5168 M_\odot$  WD with  $\dot{M}_{\text{acc}} = 1.0 \times 10^{-8} M_\odot \text{ yr}^{-1}$  starting from a cold WD of  $\log T_c$  (K) = 6.6017 which is raised to 6.9355 after only successive 60 hydrogen shell flashes (the WD mass increases to  $0.5235 M_\odot$ ).

Epelstain et al. (2007) also showed that the initially hot (cold) WD of  $T_c = 5 \times 10^7$  K ( $0.5 \times 10^7$  K) cools down (becomes hot), after the  $0.65 M_\odot$  WD experienced  $\sim 3000$  shell flashes ( $10^8 \text{ yr}$ ) with  $\dot{M}_{\text{acc}} = 1 \times 10^{-9} M_\odot \text{ yr}^{-1}$ . In the both cases of hot and cold WDs,  $T_c$  seems to approach a single value of  $\sim 1.5 \times 10^7$  K, which is much lower than our results of  $3.5 \times 10^7$  K, probably because they did not include heat balance of the core between gravitational energy release and neutrino loss, and because of some difficulties in their numerical code (see Kato et al. (2017c) for more details).

In these evolution calculations (except for Townsley & Bildsten (2004)), the flash properties such as the recurrence period, flash strength, and amount of mass-loss drastically changed in successive shell flashes (e.g., Epelstain et al. (2007) and Hillman et al. (2016)). To avoid such an initial-model dependency, we have started a calculation from an initial model close to a thermal equilibrium as done in Kato et al. (2017b).

Recurrent novae are one of the candidate of Type Ia supernova progenitors (Hachisu et al. 1996; Hachisu et al. 1999b; Hachisu et al. 1999a; Kato & Hachisu 2012). The mass-accreting WD grows its mass toward the Chandrasekhar mass limit. In such WDs the central temperature gradually increases keeping the equilibrium temperature as high as  $> 10^8$  K for  $M_{\text{WD}} > 1.3 M_\odot$  (e.g. Wang et al (2017); Wu et al. (2017)). In such a binary evolution, the mass retention efficiency is an essentially important factor. If we adopt a very low initial temperature ( $\sim 10^7$  K) such as those assumed in Prialnik & Kovetz (1995), Yaron et al. (2005), Starrfield et al. (2012), Wolf et al. (2013), and Chen et al. (2019), some of which are depicted in figure 3, the resultant nova properties and mass retention efficiency would be very different. For a cooler WD the flash is stronger and then the mass retention efficiency is estimated to be smaller than in a realistic (equilibrium) case for a long-term binary evolution. It affects the long-term binary-evolution scenarios toward type Ia supernovae.

## 7 Conclusions

Our main results are summarized as follows.

1. In a long-term cataclysmic binary evolution, the WD interior is adjusted to the mass accretion, and the central temperature is not a free parameter. We calculated such a WD interior and obtained the ignition mass, WD radius, and WD central temperature for various WD masses and mass-accretion rates.
2. In classical novae, which correspond to the case of low mass-accretion rates, its WD interior is relatively cool and the ignition mass is larger. The envelope is strongly degenerated, thus, a stronger shell flash is expected. In recurrent novae, which correspond to massive WDs with high mass-accretion rates, its envelope is less or non-degenerated. Thus, the shell flash is relatively weaker. Even if the WD masses are the same, their outburst properties are very different between high (recurrent novae) and low (classical novae) accretion rates.
3. The steady-state approximation is adequate to follow classical nova outbursts but not for recurrent novae, because the gravitational energy release rate  $L_G$  sub-

stantially contributes to change the envelope structures in recurrent novae.

- The characteristic properties of visual and X-ray light curves of V2491 Cyg are explained with a sequence of steady-state wind/static solutions. We present a model of a cold  $1.36 M_{\odot}$  WD with the envelope chemical composition of Ne nova 2. The optical light curve is explained by free-free emission from the plasma outside the photosphere in the early phase. The X-ray light curve is reproduced by blackbody fluxes from the WD photosphere, followed by emission from expanding hot ejecta.

## Acknowledgments

We thank the anonymous referee for useful comments that improved the manuscript.

## References

- Brandi, E., Quiroga, C., Mikołajewska, J., Ferrer, O. E., & García, L. G. 2009, *A&A*, 497, 815
- Chen, H., et al. 2019, *MNRAS*, 490, 1678
- Denissenkov, P. A., Herwig, F., Bildsten, L., & Paxton, B. 2013, *ApJ*, 762, 8
- Epelstain, N., Yaron, O., Kovetz, A. & Prialnik, D. 2007, *MNRAS*, 374, 1449
- José, J., Hernanz, M., & Isern, J. 1993, *A&A*, 269, 291
- Hachisu, I., & Kato, M. 2006, *ApJS*, 167, 59
- Hachisu, I., & Kato, M. 2009, *ApJ*, 694, L103
- Hachisu, I., & Kato, M. 2010, *ApJ*, 709, 680
- Hachisu, I., & Kato, M. 2015, *ApJ*, 798, 76
- Hachisu, I., & Kato, M. 2016a, *ApJS*, 223, 21
- Hachisu, I., & Kato, M. 2016b, *ApJ*, 816, 26
- Hachisu, I., & Kato, M. 2018a, *ApJ*, 858, 108
- Hachisu, I., & Kato, M. 2018b, *ApJS*, 237, 4
- Hachisu, I., & Kato, M. 2019a, *ApJS*, 241, 4
- Hachisu, I., & Kato, M. 2019b, *ApJS*, 242, 18
- Hachisu, I., & Kato, M. 2021, *ApJS*, 253, 27
- Hachisu, I., Kato, M., Kato, T., & Matsumoto, K. 2000, *ApJL*, 528, L97
- Hachisu, I., Kato, M., Kiyota, S., et al. 2006, *ApJL*, 651, L141
- Hachisu, I., Kato, M., & Luna, G. J. M. 2007, *ApJ*, 659, L153
- Hachisu, I., Kato, M., & Nomoto, K. 1996, *ApJ*, 470, L97
- Hachisu, I., Kato, M., & Nomoto, K. 1999a, *ApJ*, 522, 487
- Hachisu, I., Kato, M., Nomoto, K., & Umeda, H. 1999b, *ApJ*, 519, 314
- Hachisu, I., Saio, H., & Kato, M. 2016, *ApJ*, 824, 22
- Hachisu, I., Saio, H., Kato, M., Henze, M., & Shafter, A.W. 2020, *ApJ*, 902, 91
- Henze, M. et al. 2018, *ApJ*, 857, 68
- Hillman, Y., Prialnik, D., Kovetz, A. & Shara, M. M. 2016, *ApJ*, 819, 168
- Iben, I., Jr. 1982, *ApJ*, 259, 244
- Iglesias, C. A., & Rogers, F. J. 1996, *ApJ*, 464, 943
- Iijima, T. 2009, *A&A*, 505, 2871
- Kato, M. 1983, *PASJ*, 35, 507
- Kato, M. 1985, *PASJ*, 37, 19
- Kato, M. 1999, *PASJ*, 51, 525
- Kato, M., & Hachisu, I. 1994, *ApJ*, 437, 802
- Kato, M., & Hachisu, I. 2009, *ApJ*, 699, 1293
- Kato, M., & Hachisu, I. 2012, *Bull.Astr.Soc.India*, 40, 393
- Kato, M., & Hachisu, I. 2020, *PASJ*, 72, 82
- Kato, M., Hachisu, I., & Henze, M. 2013, *ApJ*, 779, 19
- Kato, M., Saio, H., Hachisu, I., & Nomoto, K. 2014, *ApJ*, 793, 136
- Kato, M., Hachisu, I., & Saio, H. 2017c, in *Proceedings of the Palermo Workshop 2017 on “The Golden Age of Cataclysmic Variables and Related Objects - IV”*, ed. F. Giovannelli et al. (Trieste: SISSA PoS), 315, 56
- Kato, M., Saio, H., & Hachisu, I. 2017a, *ApJ*, 838, 153
- Kato, M., Saio, H., & Hachisu, I. 2017b, *ApJ*, 844, 143
- Kato, M., Saio, H., & Hachisu, I., 2020, *ApJ*, 892, 15
- Kato, M., et al. 2016, *ApJ*, 830, 40
- Knigge, C., Baraffe, I., & Patterson, J. 2011, *ApJS*, 194, 28
- Munari, U., Siviero, A., & Dallaporta, S. 2011, *New Astronomy*, 16, 209
- Nakano, S., Beize, J., Jin, Z. -W., et al. 2008, *IAU Circular*, 8934, 1
- Ness, J.-U., Osborne, J.P., Dobrotka, A., et al. *ApJ*, 733, 70
- Ness, J.-U., et al. 2007, *ApJ*, 665, 1334
- Page, K.L., Osborne, J.P., Evans, P.A., et al., 2010, *MNRAS*, 401, 121
- Pagnotta, A., & Schaefer, B. E. 2014, *ApJ*, 788, 164,
- Piersanti, L., Cassisi, S., Iben, I. Jr., & Tornambe, A. 2000, *ApJ*, 535, 932
- Prialnik, D., & Kovetz, A., 1995, *ApJ*, 445, 789
- Sala, G., & Hernanz, M. 2005, *A&A*, 439, 1061
- Starrfield, S., et al. 2012, *BASI*, 40, 419
- Sugimoto, D., & Fujimoto, M. Y. 1978, *PASJ*, 30, 467
- Sun, B., et al. 2020, *MNRAS*, 499, 3006
- Takei, D. et al. 2009, *ApJL*, 2009, 697, L54
- Takei, D. et al. 2011, *PASJ*, 63, S729
- Tomov, T., Mikołajewski, M., Brozek, T., et al. 2008, *ATel*, 1485, 1
- Townsley, D. M., & Bildsten, L. 2004, *ApJ*, 600, 390
- Warner, B. 1995, *Cataclysmic variable stars*, Cambridge, Cambridge University Press
- Wang, B., Podsiadlowski, P., & Han, Z. 2017, *MNRAS*, 472, 1593
- Wolf, W. M., Bildsten, L., Brooks, J., & Paxton, B. 2013, *ApJ*, 777, 136, (Erratum: 2014, *ApJ*, 782, 117)
- Woodward, C. E., Gehrz, R.D., Jones, T.J., Lawrence, G.F., & Skrutskie, M.F. 1997, *ApJ*, 477, 817
- Wu, C., Wang, B., Liu, D. & Han, Z. 2017, *A&A*, 604, A31
- Yaron, O., Prialnik, D., Shara, M.M., & Kovetz, A. 2005, *ApJ*, 623, 398
- Zemko, P., Mukai, K., & Orio, M. 2015, *ApJ*, 807, 61